

# Application of three-dimensional weights of evidence in modeling concealed ore deposits: Case study of a porphyry Cu deposit in the Urmia-Dokhtar magmatic belt of Iran

Ehsan Farahbakhsh<sup>1,\*</sup>, Ardeshir Hezarkhani<sup>1</sup>, Taymour Eslamkish<sup>1</sup>, Abbas Bahroudi<sup>2</sup>, Rohitash Chandra<sup>3,4</sup>

*424, Hafez Ave., Tehran, Iran*

---

## Abstract

Given the challenges in data acquisition and modeling at the stage of detailed exploration, developing a prospectivity model particularly for disseminated ore deposits is difficult. Recent work has shown that the weights of evidence-based modeling has good potential for discovering of such deposits. In our approach, the qualitative geological and quantitative geochemical data obtained from boreholes are used to create a three-dimensional prospectivity model of a porphyry Cu deposit within the Urmia-Dokhtar magmatic arc, Iran. This prospectivity model is created using the weights of evidence method which is further extended for a three-dimensional (3D) space. We demonstrate that

---

\*Corresponding author

*Email address:* [e.farahbakhsh@aut.ac.ir](mailto:e.farahbakhsh@aut.ac.ir) (Ehsan Farahbakhsh)

<sup>1</sup>Department of Mining and Metallurgical Engineering, Amirkabir University of Technology (Tehran Polytechnic), Tehran, Iran

<sup>2</sup>School of Mining Engineering, College of Engineering, University of Tehran, Tehran, Iran

<sup>3</sup>EarthByte Group, School of Geosciences, University of Sydney, Sydney, Australia

<sup>4</sup>Centre for Translational Data Science, University of Sydney, Sydney, Australia

this method has the ability of integrating qualitative and quantitative exploration criteria in a 3D space based on the metallogenic model of the study area through prospecting for a concealed ore body. The geological data used in this study, include lithology, alteration and rock origin data. The results indicate a high correlation between monzodiorite units, silicific alteration and as expected volcanic rocks and the Cu mineralization. The input evidential models are integrated using the weights of evidence and three models including posterior probability, uncertainty and studentized posterior probability are created. The anomalous voxels in probability models are determined using concentration-volume fractal models and validated by prediction-area plots. The results show that the posterior probability model is more efficient through discovering Cu mineralization-bearing voxels, but the studentized posterior probability model is more reliable because of the effect of uncertainty in determining the voxel values. Using the Python scripts enclosed to this study, the same procedure can be implemented for exploring concealed ore bodies in other regions and locating potential zones in depth.

*Keywords:* Three-dimensional prospectivity modeling, Weights of evidence, Porphyry Cu, Urmia-Dokhtar magmatic arc

---

## **1. Introduction**

The shortage of surficial ore deposits has led the human into prospecting for concealed deposits in depth. Traditional exploration methods are becoming inefficient and costly in the case of this type of deposits over time. Mineral prospectivity mapping methods have been applied for exploring near-surface ore deposits, particularly in regional scale in past decades (Brown et al.,

2000; Carranza et al., 2005; Carranza and Sadeghi, 2010; Chen and Wu, 2017; Rodriguez-Galiano et al., 2015; Xiong and Zuo, 2018; Zuo et al., 2011). These methods have been well developed and categorized as knowledge- and data-driven methods (Cheng and Agterberg, 1999; Manap et al., 2013; Porwal et al., 2003). They have been usually used for detecting ore deposits in a two-dimensional environment and managed in geographical information systems (GIS) (Carranza et al., 2008; Carranza and Laborte, 2015; Knox-Robinson, 2000; Porwal et al., 2010).

Concealed ore deposits usually show weak exploration signals on the surface; therefore, there is a need to develop two-dimensional (2D) mineral prospectivity mapping methods in a three-dimensional (3D) space to benefit these methods for in-depth exploration of mineral resources. 3D modeling, analysis and visualization facilitate the perception of key spatial factors in mineralization, ore genesis, and geologic evolution in addition to target appraisal (Carranza, 2009; Li et al., 2018; Mao et al., 2019; Payne et al., 2015; Zuo et al., 2016). The ability of 3D modeling to provide a reliable spatial model is completely dependent on the quality of input datasets, modeling techniques, expert knowledge and the complexity of the geological setting (Fallara et al., 2006; Houlding, 1994; Jessell et al., 2014; Lindsay et al., 2012; Liu et al., 2016). A comprehensive metallogenic model helps geometric modeling and spatial analysis through enhancing the reliability of 3D models.

Some of the methods developed in recent years have focused on 3D space, known as 3D mineral prospectivity modeling methods (Hu et al., 2018; Li et al., 2015; Mao et al., 2019; Nielsen et al., 2015; Xiao et al., 2015; Yuan et al., 2014). These methods can be applied with other modeling methods,

such as geostatistics which are used for modeling drilling data and detecting deep-seated ore deposits in both regional and local scales. Regional-scale 3D mineral prospectivity modeling and quantitative assessment is rarely feasible, because required public-domain datasets with consistent coverage over large areas are not available (Xiao et al., 2015). One of the advantages of 3D mineral prospectivity modeling to geostatistics is the ability of integrating different types of qualitative and quantitative exploration data rather than modeling concentration of an individual geochemical element. Some of the exploration datasets, such as qualitative geological drilling data are gathered by spending high amount of time and money, which are surprisingly ignored at the stage of detailed exploration due to the lack of technique for combining such data with important quantitative data. 3D mineral prospectivity modeling method can integrate such data and provide an efficient model for optimizing the process of selecting new drilling locations and planning the exploitation of an ore reserve.

Using 3D mineral prospectivity modeling, useful geological, geochemical and geophysical data are integrated according to the known dispersion of mineralization in a modeling space. The result of this process is a formulated 3D model which presents a quantitative assessment of the probability of detecting a target mineralization based on exploration criteria. The exploration criteria must include all the factors which control target mineralization in a study area (Yuan et al., 2014). They can be used to create 3D evidential models and converted into binary models as input models for the modeling process.

The weights of evidence method is based on Bayes' rule (Xiao et al., 2015) and



has been effectively used for 2D mineral prospectivity mapping (e.g., Carranza (2004); Pazand and Hezarkhani (2014); Porwal et al. (2010); Zeghouane et al. (2016)). It has a number of advantages compared to other simpler or even more complicated data-driven methods. The weights of evidence represent the degree of correlation between a target mineralization and a particular model or pattern created under specific conditions known as an evidence (Agterberg et al., 1990; Bonham-Carter et al., 1989; Carranza, 2004; Cheng and Agterberg, 1999; Yuan et al., 2014).

In this study, we develop and demonstrate the application of the weights of evidence in a 3D space for modeling a porphyry copper (Cu) deposit located in southeast of Iran within a magmatic arc called Urmia-Dokhtar. We use borehole data comprised of qualitative geological and quantitative geochemical data, which provide input 3D evidential models. The models created using 3D weights of evidence include posterior probability, uncertainty, and studentized posterior probability models. The Python scripts used for implementing the weights of evidence method in a 3D space are released enclosed to this study. Beside this method, we use concentration-volume fractal models and prediction-area plots to evaluate and validate our models. Eventually, we provide an estimate of the reserve and potential places for future drilling.

## **2. Geological setting of the study area**

The study area is located within a magmatic arc subdivision called Urmia-Dokhtar where extensive Tertiary to Plio-Quaternary intrusive and extrusive units are exposed in a NW–SE trend (Figure 1). In several studies, a subduction-related magmatic model is suggested for the Urmia-Dokhtar

magmatic arc, which is known to be result of the closure of the Neo-Tethys ocean between Arabian and Eurasian plate (Berberian and Berberian, 1981; Omrani et al., 2008). In general, this magmatic arc involves two major mineralization regions of Chahar Gonbad to the southeast and Sungun to the northwest. The dominant type of mineralization is porphyry Cu which is associated with Eocene, Pliocene and Quaternary granitoids, plutonic bodies and volcanic rocks. Our study area is located in the Chahar Gonbad region in the southeast of Iran.

The major lithological units in the study area comprise volcanic and subvolcanic complexes, and intrusive bodies. The volcanic rocks cover most of the study area and consist of Eocene andesite, dacite and rhyodacite associated with tuff breccias (Abedi et al., 2014). The intrusive bodies include granite to diorite dispersed in the south to southwest of the study area (Figure 2). As shown in Figure 2, most of the geological units have been altered due to hydrothermal processes. The most intensive alteration has occurred in subvolcanic rhyodacite units. The major trend of these units and hydrothermal dissemination is NE–SW. It is known that there is a comprehensive correlation between hydrothermal zones and faults (Lu et al., 2016); therefore, it is assumed that the alteration zones have been controlled by the faults and fractures in the study area. However, the Cu-bearing mineralization zones are mainly associated with azurite and malachite stockwork veins with minor chalcopyrite as inclusions within quartz (Abedi et al., 2014).

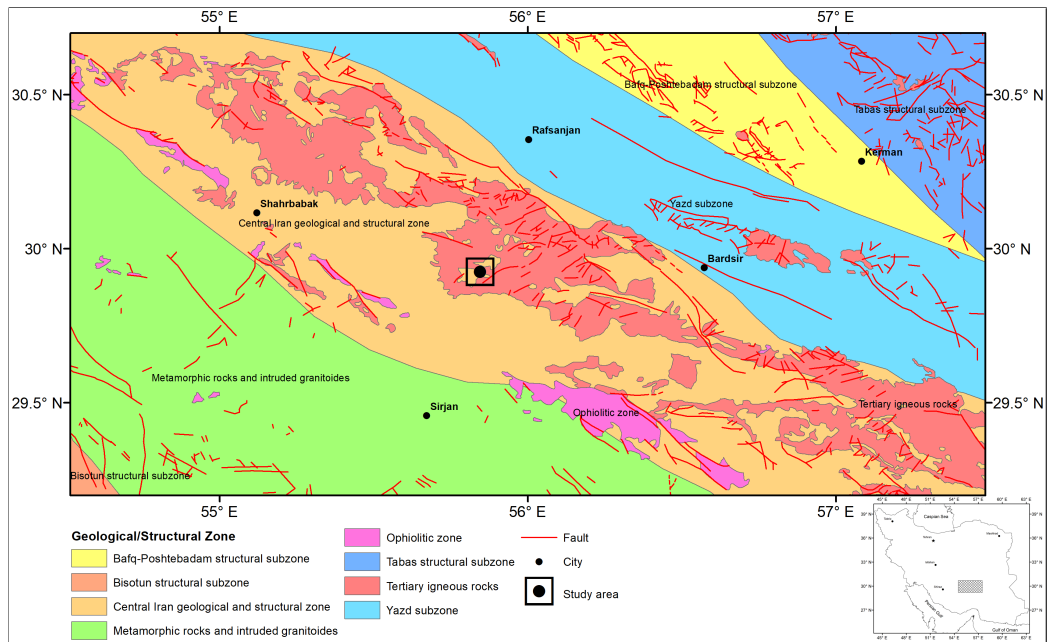


Figure 1: A portion of the Chahar Gonbad region located in the southeast of Iran within the Urmia-Dokhtar magmatic arc. The study area is shown at the center of the map in a black square.

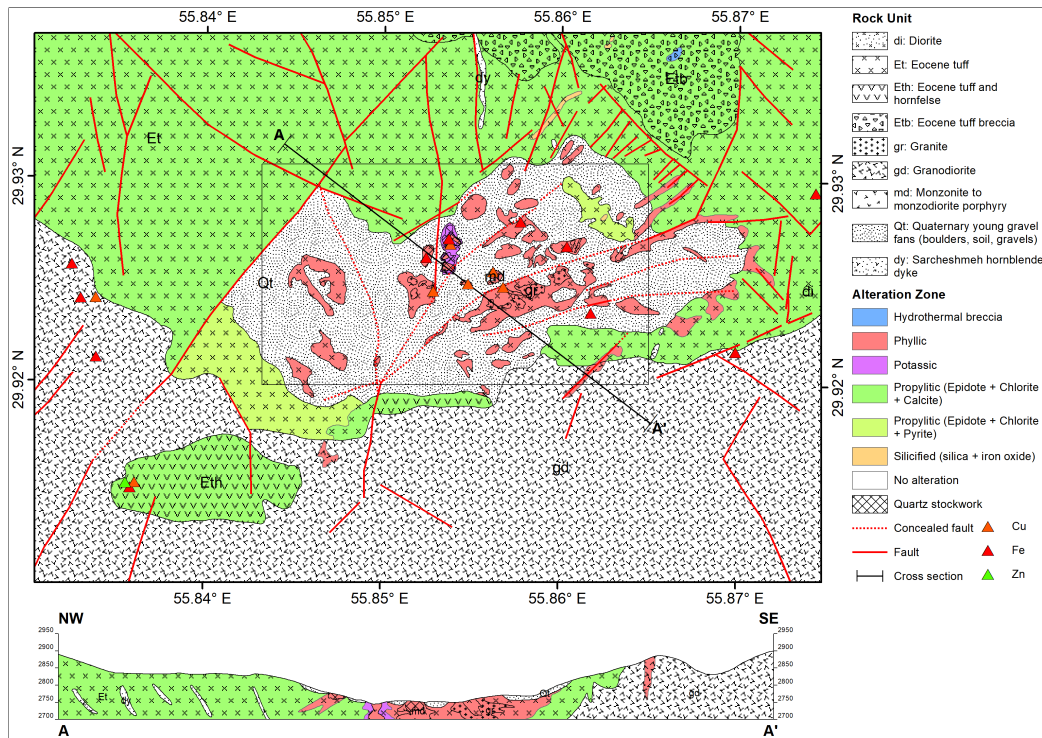


Figure 2: Detailed geological and alteration map of the study area along with a cross-section drawn over the study area intersecting some of the mineral occurrences. The black rectangle shows the target area.

### 3. Materials and methods

#### 3.1. *Drilling data*

In this study, we use drilling data that include geological and geochemical data obtained from 113 boreholes. The location of borehole collars on the geological map can be found in Figure 3. The polygon drawn around borehole collars using convex hull algorithm shows the super-face of the modeling space. The geological data used for creating 3D geological evidential models involve lithology, alteration, and rock origin information. In addition to Cu concentration values which is used for creating the target ore body, we use other geochemical data including concentration values of Fe, Mo, and Zn for creating 3D geochemical evidential models. These elements are usually applied through prospecting for porphyry Cu deposits (Farahbakhsh et al., 2019). The 3D strip-logs of the geological and geochemical data are shown in Figures 4 and 5, respectively.

#### 3.2. *3D modeling*

##### 3.2.1. *Geological modeling*

We use an interpolation method known as lateral blending for interpolating qualitative geological data including lithology, alteration and rock origin in a 3D space. This method available with the RockWorks software package (RockWorks17, 2019b), horizontally extrudes data and randomizes correlations within the mid-zone region. The method produces transgressive or regressive correlations that are similar to what a geologist would hand-draw (RockWorks17, 2019a; Shishaye et al., 2019). The limitation of the method



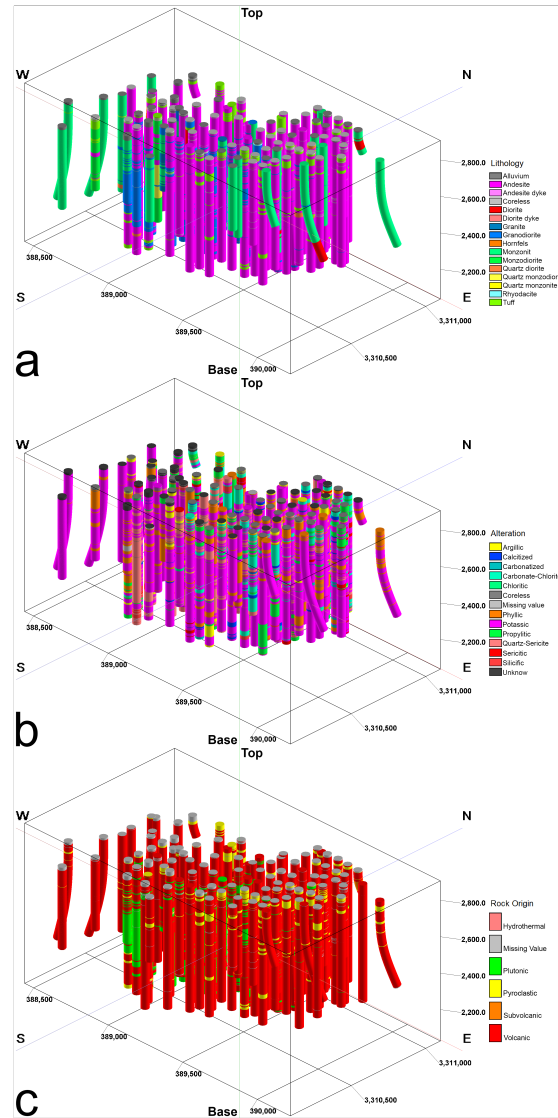


Figure 4: 3D strip-logs of the geological data including a) lithology; b) alteration; and c) rock origin.

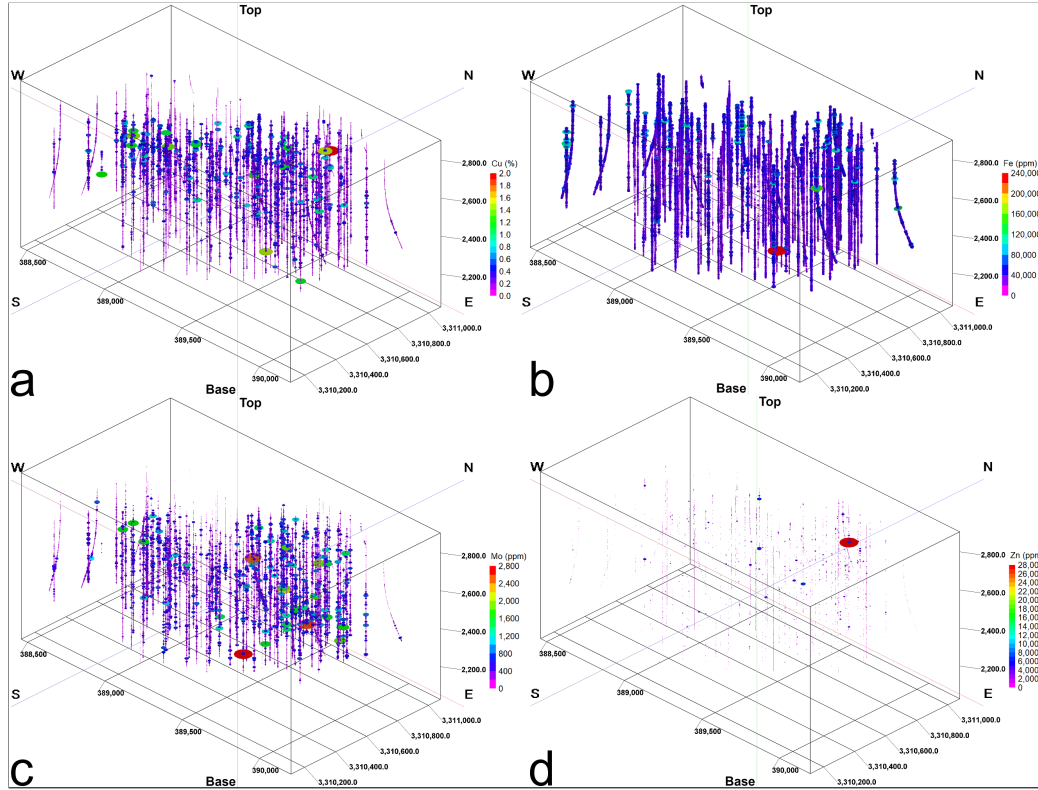


Figure 5: 3D strip-logs of the geochemical data including a) Cu; b) Fe; c) Mo; and d) Zn concentration values. The size and color of cylinders shown along the boreholes are proportionate to the intensity of concentration values. Highly positive skewed Zn concentration values yields a poor illustration of the relevant 3D strip-logs.



is due to randomization of the mid-zone, which means that slightly different models are produced each time the model runs.

### *3.2.2. Geochemical modeling*

The geochemical anomalies of iron, molybdenum and zinc (Fe, Mo, and Zn) are key indications of porphyry Cu mineralization in the study area. We use the inverse-distance anisotropic modeling method which is one of the different kinds of the inverse-distance algorithm for interpolating geochemical data in a 3D space. Using inverse-distance in general, we assign a voxel node value based on the weighted average of neighboring data points, and the value of each data point is weighted according to the inverse of its distance from the voxel node, taken to a power. The greater the value of the exponent, the less influence distant control points will have on the assignment of the voxel node value (RockWorks17, 2019a; Zuo et al., 2016).

Using the inverse-distance anisotropic method, we look for the closest control point in each 90-degree sector around the node. In this study, the weighting exponent is set to 2, experimentally. The directional search can improve the interpolation of voxel values that lie between data point clusters, and can be useful for modeling borehole-based data, and particularly for stratiform deposits. The quadrant searching tends to connect the limits (highs and lows) at the same elevation.

### *3.3. Weights of evidence modeling*

Weights of evidence is a data-driven prospectivity modeling method and known as a Bayesian probabilistic method (Bonham-Carter, 1994). This method is used for estimating the posterior probability of a target ore body

under the assumption of conditional independence of input evidential models (Xiao et al., 2015). This assumption is also known as one of the weaknesses of this method (Joly et al., 2012). Using this method, prior belief of the model of a specific type of mineralization or an ore deposit in an area or space is updated in the light of other evidence such as geological, geochemical or geophysical models. An example of the prior belief is the primary model created by interpolating concentration values of the target element obtained through the boreholes. The posterior probability of mineralization  $P(M)$  after looking at data or evidence ( $E$ ) is determined via the likelihood function using Eq. 1 (Bonham-Carter, 1994):

$$P(M|E) = P(M) \frac{P(E|M)}{P(E)} \quad (1)$$

This method is simple from the computational view, and 2D weights of evidence is readily implemented in GIS packages (e.g., ArcGIS Desktop (2019); QGIS Development Team (2019)); however, implementing this method in a 3D space is more complicated. The weights of evidence method enables a user to interpret calculated positive and negative weights in geological terms intuitively. The positive and negative weights indicate the spatial association between the voxels with and without mineralization, and the presence and absence of anomalous voxels of evidential models. For example, an evidential or predictor model can be used to assess the contribution of a geological process in the formation and prospectivity of a specific type of mineralization (Xiao et al., 2015). Moreover, this method can work with a low number of training datasets compared to other data-driven or machine learning techniques. The three-dimensional weights of evidence used in this study is

similar to the traditional method applied for mineral prospectivity mapping (Bonham-Carter, 1994; Carranza, 2004), and pixels are replaced with voxels. The steps for 3D mineral potential modeling using the weights of evidence which are implemented in this study, can be summarized as shown in Figure 6 and described as follows:

- Acquiring drilling data including required geological and geochemical data;
- Creating the model of target ore body based on the Cu concentration values along the boreholes in different intervals;
- Providing 3D geological and geochemical evidential models;
- Calculating weights of evidence and other important parameters such as standard deviation and variance of the weights for different geochemical models based on a range of thresholds and for each unit of geological models;
- Determining the best threshold for converting continuous geochemical models into binary models;
- Selecting input evidential models for creating the posterior model based on the contrast and studentized contrast;
- Integrating selected evidential layers and creating 3D posterior probability, uncertainty and studentized posterior probability models;
- Validating the results.

### *3.3.1. Binarization*

One of the most important steps in prospectivity modeling based on the weights of evidence method is determining a proper threshold for converting

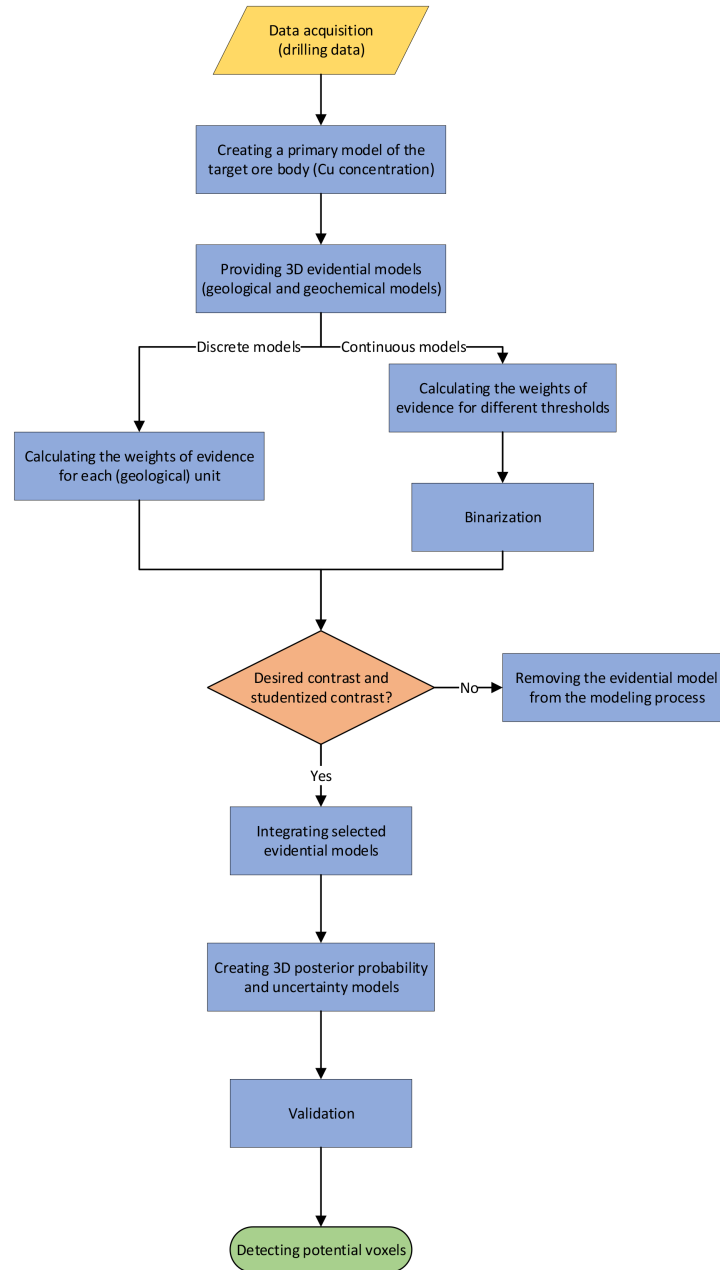


Figure 6: Methodology flowchart of this study for 3D mineral prospectivity modeling of an ore deposit using the weights of evidence method.

continuous models, such as geochemical models into binary models. In this study, we classify continuous models based on different standard deviations of the mean. Each continuous model is classified with the thresholds ranging between mean and a width of five standard deviation to the right side of the distribution function with an increment equal to half of the standard deviation. The result for each continuous model is eleven binary models. The Cu concentration values are interpolated as well as other geochemical elements, and then converted into a binary model for determining the target ore body. We calculate the positive and negative weights for each binary evidential model created by different thresholds for multiple models of the target ore body. These weights along with other important parameters such as contrast are calculated as described by Bonham-Carter (1994) and Bonham-Carter et al. (1989). Here, contrast values are used to assess the association between known mineralization voxels and evidential models. The threshold used for separating anomalous voxels of the Cu concentration is determined by checking each binary model of the Cu concentration for the maximum studentized contrast of the evidential models.

The thresholds for creating binary evidential models using continuous geochemical models are determined based on the maximum studentized contrast and the occupied percentage of the modeling space. According to the occupied percentage of the modeling space by the target ore body, we only investigate the thresholds in terms of the studentized contrast, above which anomalous voxels occupy at least 1% of the modeling space.

### 3.3.2. Posterior probability

The posterior probability model which is the result of integrating input evidential models, is generated using Bayes' equation in a log-linear form with the assumption that conditional independence applies (Bonham-Carter, 1994; Bonham-Carter et al., 1989). In this study, we use the Concentration-Volume (C-V) fractal model (Afzal et al., 2011) for determining a proper threshold for separating anomaly population of voxels from the background.

### 3.3.3. Studentized posterior probability

Using the weights of evidence enables the user to calculate the effects of uncertainty in the weights, and uncertainty due to missing information, and produce an uncertainty quantified model which is propagated in the decision making. The variances of the weights and contrast also help to determine the cutoff level at which to convert multiclass models to binary form, and to model the uncertainty of the posterior probability due to uncertainty in the weights and caused by lack of information (Bonham-Carter, 1994). In this study, the parameters required for creating the uncertainty model include standard deviation and variance of the weights, and contrast which are calculated by adapting the methods described by Bishop et al. (1975), Bonham-Carter (1994), Bonham-Carter et al. (1989) and Carranza (2004). A useful measure is to calculate the studentized value of the contrast, as a measure of the uncertainty with which the contrast is known. The studentized value  $S(C)$  is calculated as the ratio of contrast  $C$  to its standard deviation  $StD(C)$  as shown below:

$$S(C) = \frac{C}{StD(C)} \quad (2)$$

As long as the ratio is relatively large, implying that the contrast is large compared with the standard deviation, then the contrast is more likely to be real. A studentized value larger than 2, or even 1.5 is satisfactory. Due to the assumptions required for a formal statistical test, particularly the problem with the dependence of the standard deviation of contrast on the units of measurement, it is best to use this ratio in a relative, rather than an absolute sense (Bonham-Carter, 1994).

The variances of the weights can be used to calculate the variance of the posterior probability at each voxel, and to generate an uncertainty model that accompanies the posterior probability model. The square root of the total variance at each voxel equals the standard deviation. The ratio of the posterior probability to the corresponding standard deviation is called studentized posterior probability. The studentized posterior probability acts as a measure of the relative certainty of the posterior probability. The voxels where the studentized value falls below some threshold can be masked out, due to lack of confidence in the results. In this study, the threshold is determined based on the C-V fractal model.

## 4. Results

### 4.1. 3D evidential models

In this study, we use qualitative geological and quantitative geochemical data obtained from the boreholes to create 3D geological and geochemical evidential models. We later apply these models to create a 3D mineral

Parameter	Value
North-South extent	970 m
East-West extent	1,740 m
Vertical extent	890 m
Polygon area on the surface	0.8841 km <sup>2</sup>

Table 1: Geometrical parameters of the 3D modeling space.

prospectivity model. The size of each voxel in the 3D models according to the extent of the modeling space is determined  $10 \times 10 \times 10$  meters (m) and other geometrical parameters can be found in Table 1. The 3D models are inscribed in a polygon created by the convex hull algorithm based on the coordinates of the borehole collars (Figure 3). Moreover, they are restricted to a super- and sub-face based on the elevation of the borehole collars and the depth of each borehole to make sure that there are sufficient number of data points for interpolating throughout the modeling space. The total number of voxels is approximately 500,000.

#### 4.1.1. Geological models

Three different types of geological data including lithology, alteration and rock origin are used for creating 3D geological evidential models. As shown in Figure 3, we designed two cross-sections (AA' and BB') along the small and large diameters of the study area to visually investigate the correlation between the aforementioned data types and the Cu concentration. These cross-sections along with the interpolated Cu concentration anomaly zones (greater than 0.2%) are shown in Figure 7.

We used RockWorks software package RockWorks17 (2019b) for creating





3D solid models using different available geological data obtained from the boreholes. As described in section 3.2, a method called lateral blending is used to interpolate the geological data in the 3D space. Figure 8 presents the solid models created using lithology, alteration and rock origin data. Moreover, two fence diagrams in different views from each solid model are shown in Figure 9.

#### *4.1.2. Geochemical models*

We use the Cu concentration values in different intervals through the boreholes to create a primary 3D model of the target ore body concealed in depth using the inverse-distance anisotropic interpolation method which is later used as a training model. Moreover, we use Fe, Mo, and Zn concentration values for creating other geochemical evidential models. In Figure 10, anomalous voxels of these 3D geochemical models are shown. The threshold used in each model for discriminating the anomaly population from the background values are determined by the maximum studentized contrast. Further details on this can be found in the next section.

#### *4.2. Prospectivity modeling*

As explained in section 3.3, according to the results and the known cut-off grade of Cu concentration in the study area, the threshold for creating a binary model of the target ore body is determined 0.45%. Based on this threshold, the target ore body occupies 1.34% of the total modeling space which can also be considered as the prior probability (Figure 10a). The weights of evidence for different binary models based on different thresholds for Fe, Mo, and Zn concentration values are presented in Tables 2–4, re-



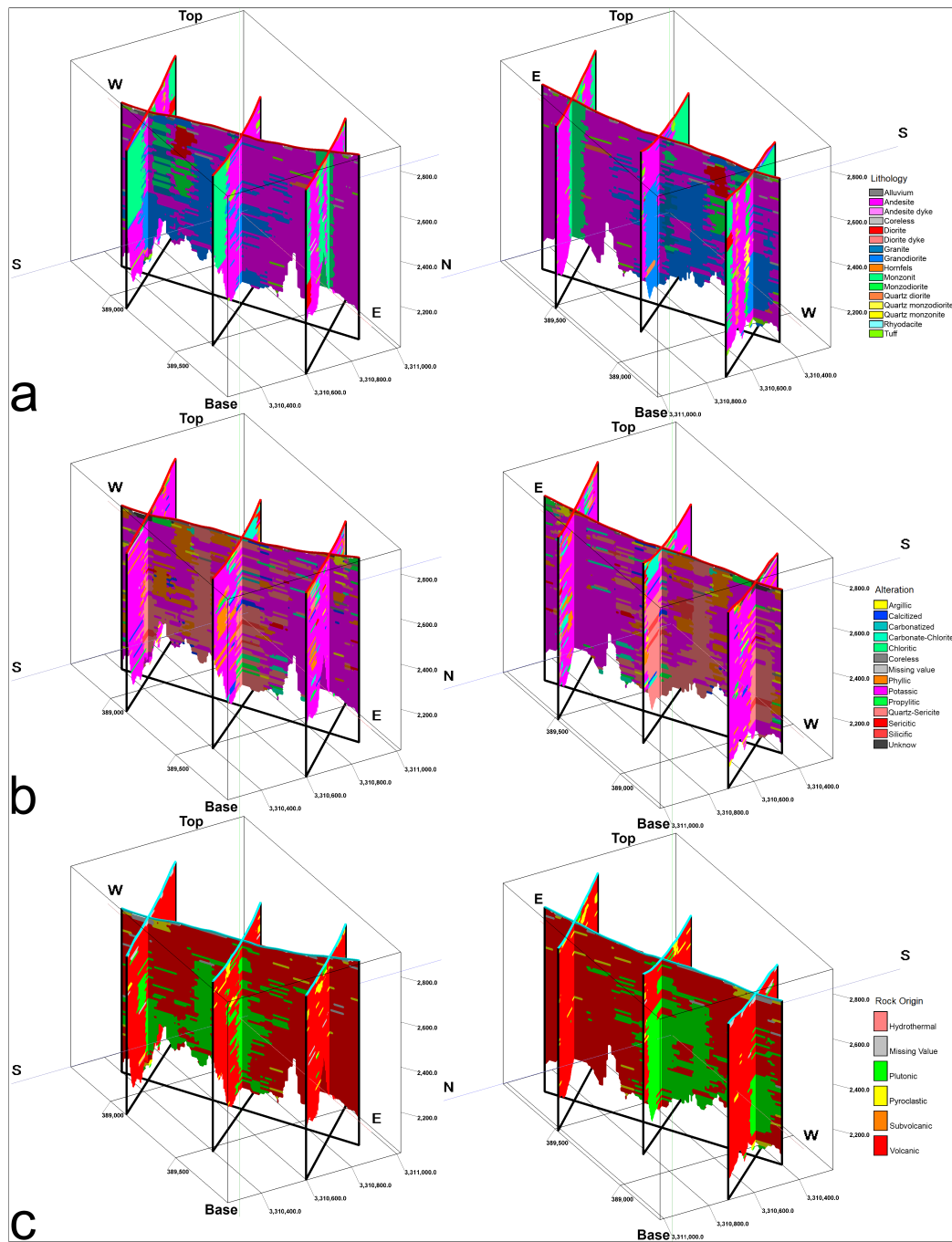


Figure 9: Fence diagrams created from solid models generated by a) lithology, b) alteration, and c) rock origin data in two different views to NW on the left and to SE on the right side.



Thresholds	Volume (m <sup>3</sup> )	Percentage	W+	Var <sup>1</sup> (W+)	StD <sup>2</sup> (W+)	W-	Var (W-)	StD (W-)	Contrast	Studentized contrast
50016.4914	260474000	52.174	0.2312	0.0001	0.0121	-0.3293	0.0003	0.0166	0.5605	27.2687
57930.7629	144319000	28.9077	0.3852	0.0002	0.0152	-0.2088	0.0002	0.0128	0.594	29.895
65845.0344	60127000	12.0437	0.8482	0.0004	0.019	-0.1949	0.0001	0.0115	1.0431	47.0363
73759.3058	24294000	4.8662	1.2902	0.0006	0.0246	-0.136	0.0001	0.0107	1.4263	53.1745
<b>81673.5773</b>	10399000	2.083	1.7728	0.001	0.0309	-0.0987	0.0001	0.0104	1.8714	<b>57.4621</b>
89587.8488	5198000	1.0412	2.1219	0.0015	0.0384	-0.0691	0.0001	0.0102	2.191	55.1311

<sup>1</sup> Variance <sup>2</sup> Standard Deviation

Table 2: Variation of the weights of evidence and other important parameters with increasing the threshold for Fe concentration values.

spectively. According to these tables, the thresholds determined for creating binary models of Fe, Mo, and Zn concentration are 81673.57, 259.93 and 2512.98 ppm, respectively. The anomalous voxels of Fe, Mo, and Zn concentration occupy 2.08, 23.81 and 1.12% of the total modeling space. The variations of contrast and studentized contrast of the mentioned elements are shown in Figure 11.

Every unit of lithology, alteration and rock origin data is considered as a binary model and the weights of evidence and other important parameters are calculated for it. The results are presented in 5. The lithology and alteration units as well as the different types of rock origin which are not found in this table show negative contrast due to low number of occupied voxels, and hence low number of common voxels with the target ore body. More details can be found in the supplementary file.

The evidential models are combined as mentioned in section 3.3 and a posterior probability model is the result. The C-V fractal model is used for determining a proper threshold through separating anomalous voxels and the background. According to the C-V chart presented in Figure 12, the voxels showing a posterior probability greater than 0.75 are considered as part of the anomalous population and the most probable places for Cu mineralization.

Thresholds	Volume (m <sup>3</sup> )	Percentage	W+	Var (W+)	StD (W+)	W-	Var (W-)	StD (W-)	Contrast	Studentized contrast
189.4115	211183000	42.3008	0.2054	0.0002	0.0136	-0.1812	0.0002	0.0141	0.3866	19.7286
<b>259.936</b>	118906000	23.8174	0.3079	0.0003	0.0173	-0.1183	0.0001	0.0119	0.4263	<b>20.2931</b>
330.4605	63859000	12.7912	0.4165	0.0005	0.0225	-0.0778	0.0001	0.0109	0.4943	19.7973
400.985	33723000	6.7549	0.5625	0.0008	0.0289	-0.0553	0.0001	0.0104	0.6177	20.1156
471.5095	18528000	3.7112	0.6151	0.0014	0.038	-0.0327	0.0001	0.0101	0.6478	16.456
542.034	10870000	2.1773	0.6778	0.0023	0.0483	-0.0214	0.0001	0.01	0.6992	14.1896
612.5585	6809000	1.3639	0.9333	0.0029	0.0543	-0.0209	0.0001	0.01	0.9541	17.2837

Table 3: Variation of the weights of evidence and other important parameters with increasing the threshold for Mo concentration values.

Thresholds	Volume (m <sup>3</sup> )	Percentage	W+	Var (W+)	StD (W+)	W-	Var (W-)	StD (W-)	Contrast	Studentized contrast
336.3968	118812000	23.7985	0.057	0.0004	0.0195	-0.0184	0.0001	0.0113	0.0754	3.3408
699.1618	50070000	10.0292	0.0876	0.0009	0.0296	-0.0102	0.0001	0.0104	0.0978	3.1137
1061.9267	28432000	5.695	0.1455	0.0015	0.0383	-0.0095	0.0001	0.0101	0.1549	3.9134
1424.6917	17507000	3.5067	0.3423	0.002	0.0444	-0.0148	0.0001	0.01	0.3571	7.839
1787.4567	11507000	2.3049	0.5239	0.0025	0.0503	-0.0161	0.0001	0.01	0.54	10.5212
2150.2217	7880000	1.5784	0.6427	0.0033	0.0576	-0.0143	0.0001	0.0099	0.657	11.2413
<b>2512.9866</b>	5595000	1.1207	0.8391	0.0039	0.0625	-0.0146	0.0001	0.0099	0.8537	<b>13.4917</b>

Table 4: Variation of the weights of evidence and other important parameters with increasing the threshold for Zn concentration values.

Lithology	Volume (m <sup>3</sup> )	Percentage	W+	Var (W+)	StD (W+)	W-	Var (W-)	StD (W-)	Contrast	Studentized contrast
Granite	4570000	0.9154	0.3096	0.0078	0.0883	-0.0033	0.0001	0.0099	0.3129	3.5208
Monzodiorite	16382000	3.2814	1.1084	0.001	0.0324	-0.0682	0.0001	0.0103	1.1766	34.6197
Monzonite	105457000	21.1235	0.2664	0.0004	0.0188	-0.0846	0.0001	0.0115	0.351	15.9568
Tuff	15864000	3.1776	0.0244	0.0029	0.0543	-0.0008	0.0001	0.01	0.0252	0.456
<b>Alteration</b>										
Argillic	7889000	1.5802	0.1443	0.0053	0.0727	-0.0025	0.0001	0.0099	0.1467	2.0001
Calcitized	4483000	0.898	0.3677	0.0075	0.0868	-0.004	0.0001	0.0099	0.3717	4.2561
Phyllic	45858000	9.1855	0.1427	0.0009	0.0302	-0.0156	0.0001	0.0103	0.1583	4.9619
Potassic	328661000	65.8321	0.0707	0.0001	0.0117	-0.1514	0.0003	0.018	0.222	10.348
Silicific	4231000	0.8475	1.2661	0.0035	0.0595	-0.0209	0.0001	0.0099	1.287	21.3234
<b>Rock origin</b>										
Volcanic	435409000	87.2142	0.0399	0.0001	0.0103	-0.3229	0.001	0.032	0.3628	10.7988

Table 5: Variation of the weights of evidence and other important parameters with different lithology and alteration units and volcanic rocks as a rock origin.

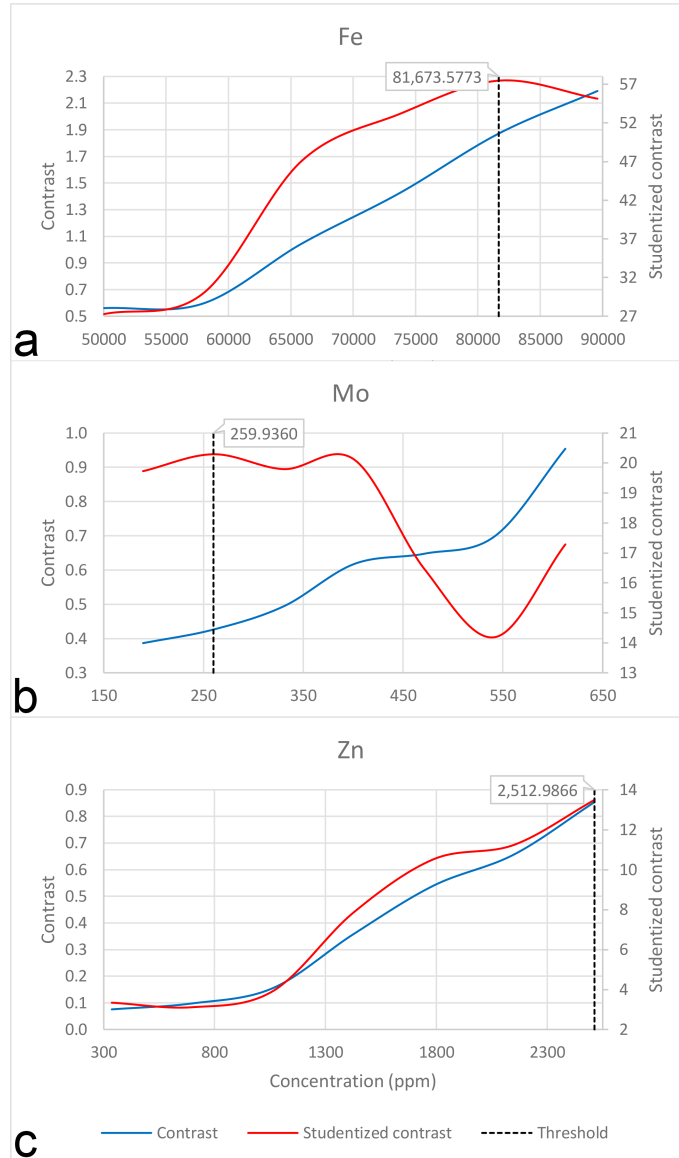


Figure 11: Variations of the contrast and studentized contrast with concentration values of a) Fe, b) Mo and c) Zn, drawn from the data in Tables 2–4.



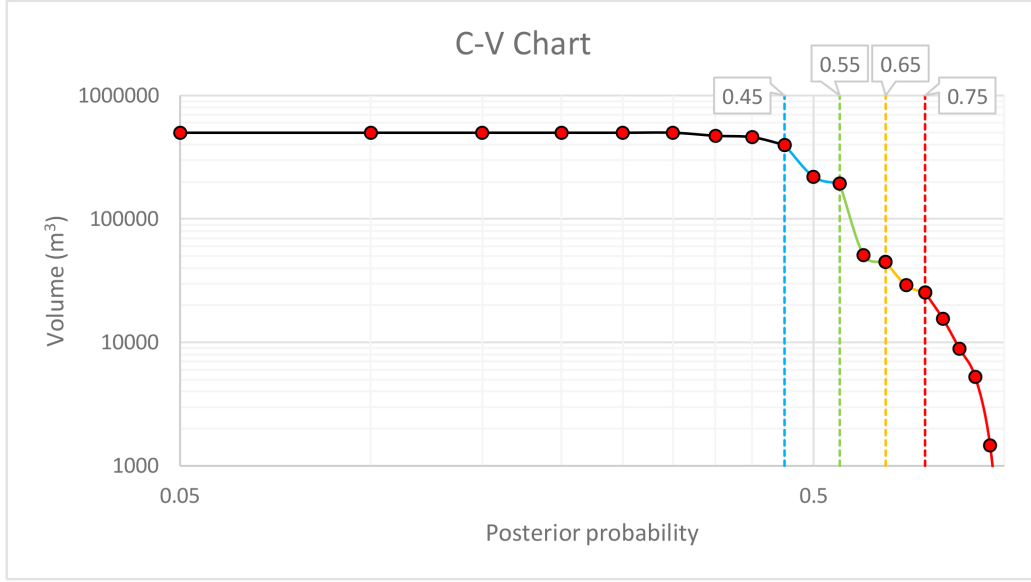


Figure 12: C-V chart of the posterior probability of Cu mineralization in the modeling space.

These voxels occupy 3.11% of the modeling space. In Figure 13, the posterior probability model and the anomalous voxels are shown.

#### 4.3. Uncertainty

The total variance of each voxel is given by summing the variances of the weights of evidence, which can be considered as a parameter for determining the uncertainty of each voxel. In Figure 14a, the 3D model of the total variance is shown. According to the histogram of the total variance shown in Figure 14, there is a gap between the bins, and the voxels with values greater than 1 are considered as the anomalous voxels which are shown in Figure 14b. The anomalous voxels include 3.28% of the total modeling space.

The 3D model of the studentized posterior probability and the anomalous voxels are shown in Figure 16. We used C-V fractal model for separating the

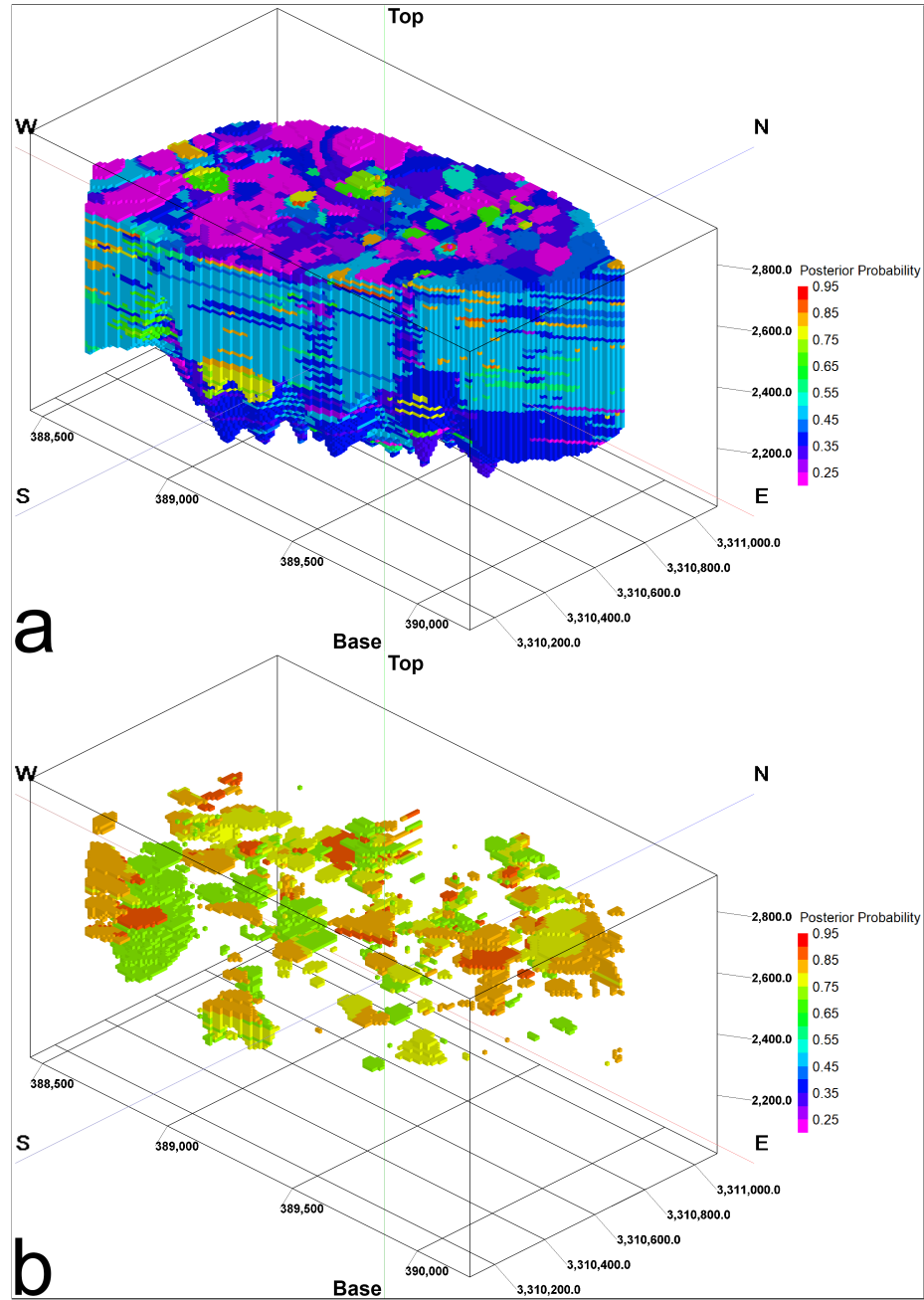


Figure 13: a) Posterior probability model of the Cu mineralization; b) anomalous voxels extracted based on the threshold determined by the C-V fractal model equal to 0.75.

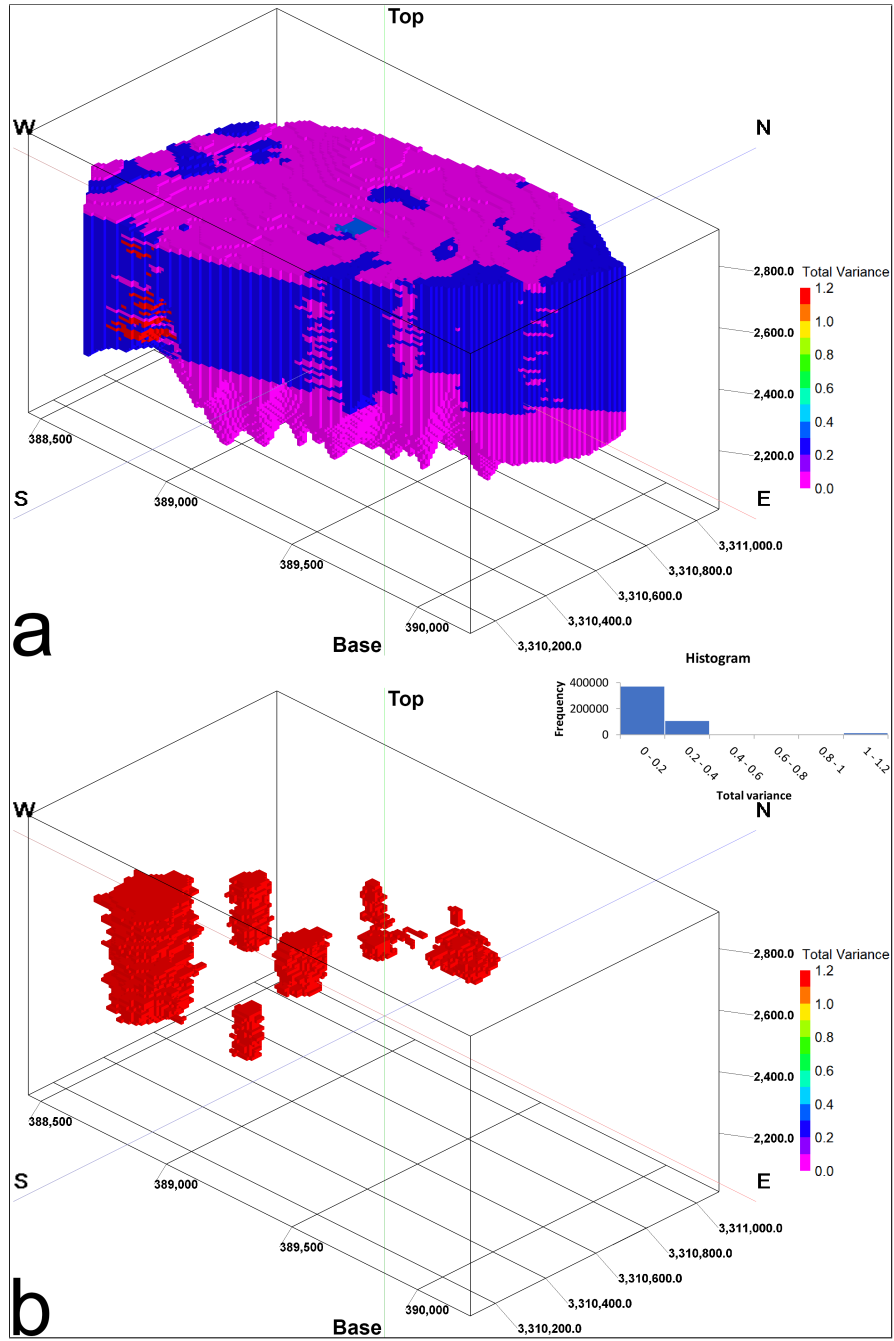


Figure 14: a) 3D model of the total variance and relevant histogram; b) anomalous voxels of the total variance which are greater than 1.

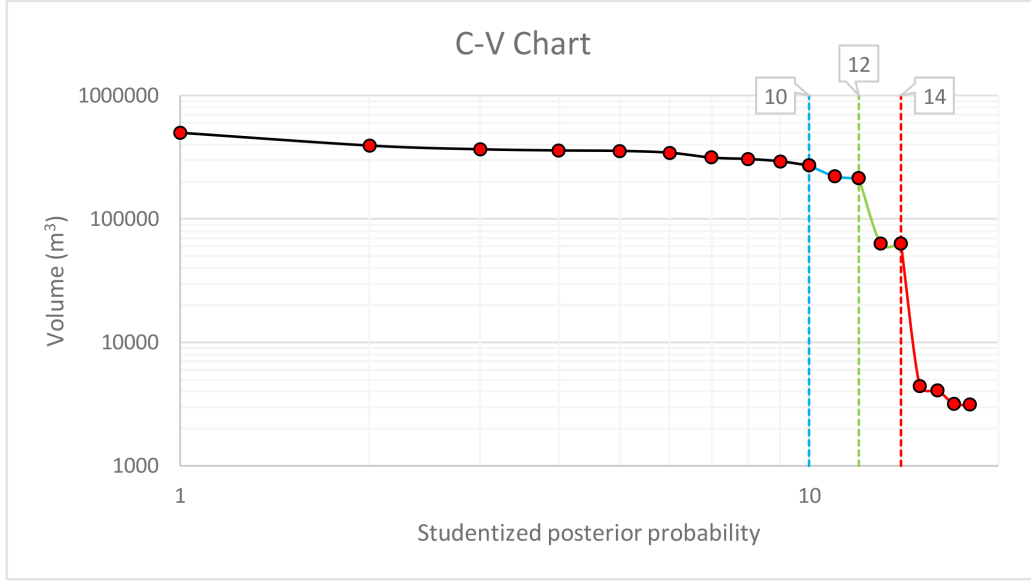


Figure 15: C-V chart of the studentized posterior probability of the Cu mineralization in the modeling space.

anomalous voxels from the background. According to the relevant chart shown in Figure 15, the voxels with values greater than 14 are considered anomalous which include 0.88% of the total modeling space.

#### 4.4. Validation

The prediction-area (P-A) plot is used in order to quantitatively validate the results obtained from the probability models. In a P-A plot, the cumulative percentage of predicted mineralization and the corresponding cumulative occupied volume, with respect to the total volume, are shown against the prospectivity values. Therefore, the prediction ability of a prospectivity model and its ability to delimit the modeling space for further exploration and drilling are evaluated in a scheme. The P-A plot shows a curve of the percentage (prediction rate) of known mineralization and a curve of the per-

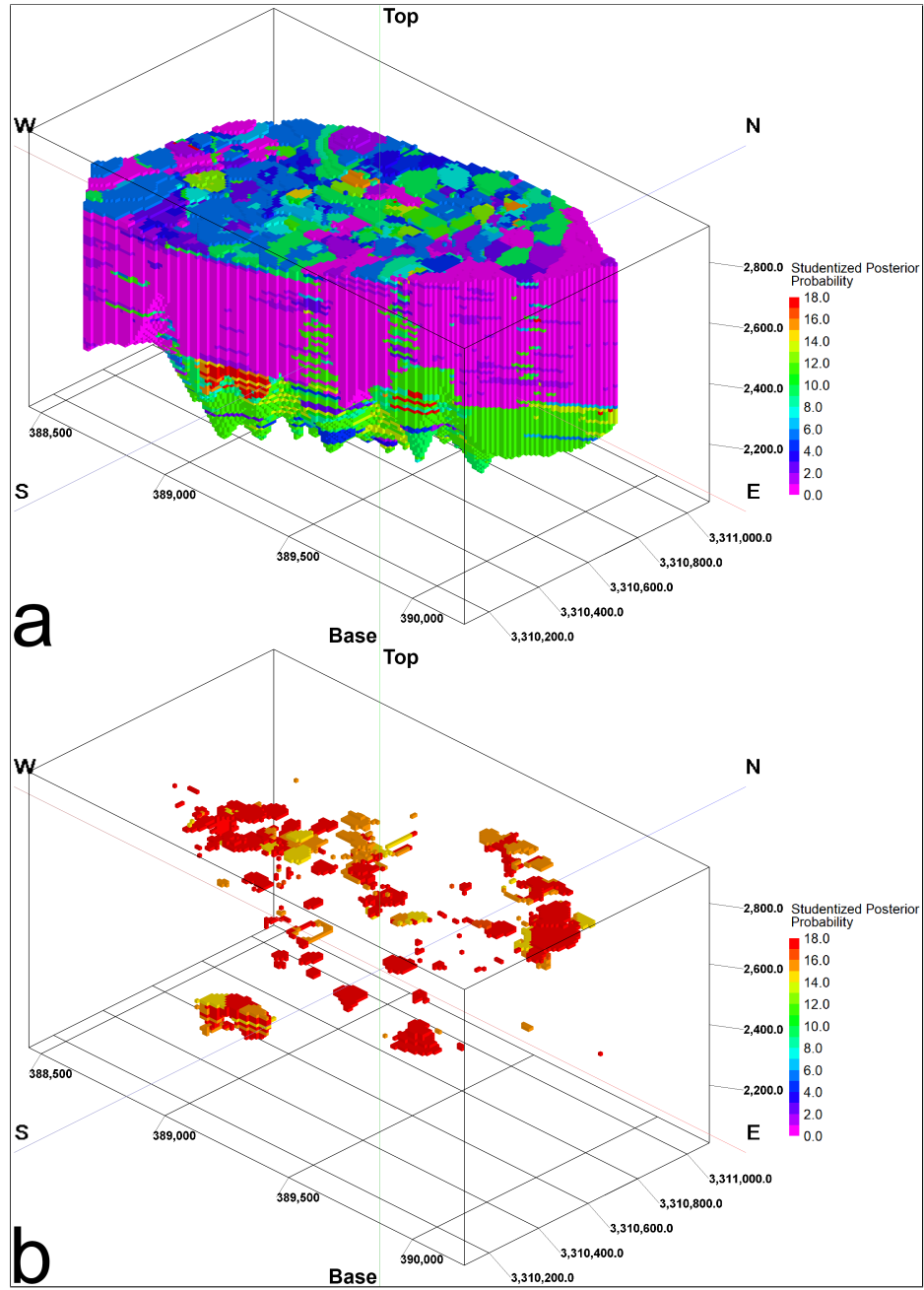


Figure 16: a) Studentized posterior probability model of the Cu mineralization; b) anomalous voxels extracted based on the threshold determined by the C-V fractal model equal to 14.

centage of occupied volume corresponding to the classes of a prospectivity model. When an intersection point of the two curves is at a higher place, it portrays a small volume containing a large number of mineralization-bearing voxels. Furthermore Farahbakhsh et al. (2019), objectively chooses a better model to give priority for mineral exploration. The comparison of the prediction rates in the P-A plots, which are shown in Figure 17, indicates the importance of analyzing the predictability of prospectivity models. We compared two prospectivity models including the posterior probability and studentized posterior probability models. It is noteworthy that for assigning probabilistic values to both models, in terms of prospecting for Cu mineralization and distribution of the voxel values between 0 and 1, they are transformed to a fuzzy space using a logistic function (Yousefi and Nykänen, 2016). This transformation not only results in better discrimination of the anomalies from the background level, but also improves the prediction rate of the known places of mineralization.

## 5. Discussion

In this study, we used two different types of drilling data including the qualitative geological and the quantitative geochemical data obtained from 113 boreholes through creating a 3D prospectivity model of Cu mineralization in the study area. The geological data comprise three types of data including lithology, alteration and rock origin. There are 15 different types of lithology in the modeling space according to the drilling data, while the diversity of lithology on the surface is less (Figures 2 and 4a). Among these lithology types, four lithology types including granite, monzodiorite, monzonite and

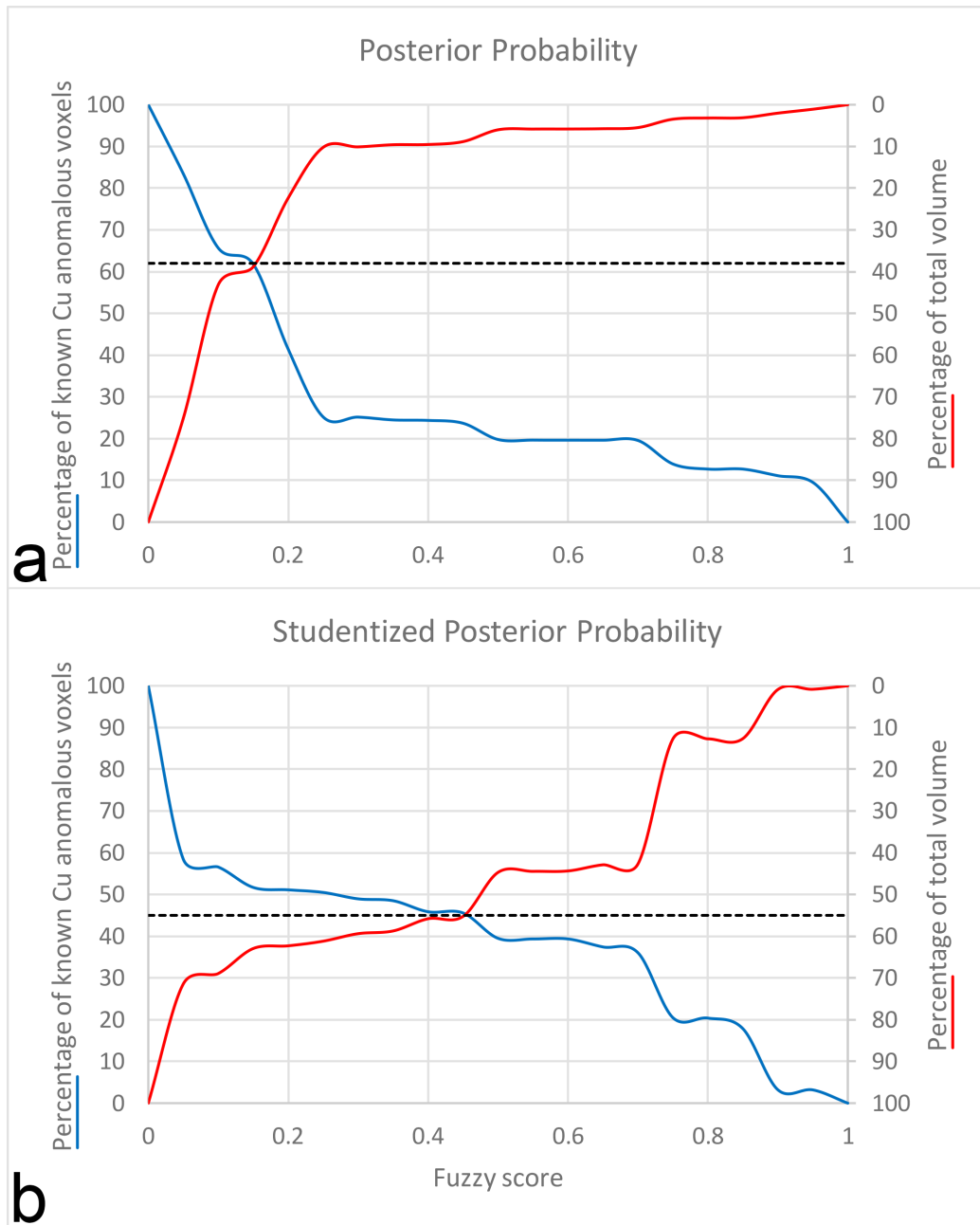


Figure 17: P-A plots for a) the posterior probability and b) the studentized posterior probability prospectivity models.

tuff show positive contrast and studentized contrast (Table 5) which were used as input binary models to the modeling process. The monzodiorite units which involve about 3% of the modeling space show the highest contrast and studentized contrast indicating high correlation of this lithology type with the Cu mineralization in the modeling space. The monzonite units which involve greater than 21% of the modeling space are in the second place of the highest studentized contrast and show low contrast value, but a high studentized contrast indicates low uncertainty of these units in terms of association with the Cu mineralization in the modeling space. The granite units which involve less than 1% of the modeling space show low contrast value, but a relatively high studentized contrast value which is much lower than the monzodiorite and monzonite units. The tuff units which involve about 3% of the modeling space and as expected, they show low contrast and studentized contrast indicating the weak association with the Cu mineralization in the modeling space.

According to the drilling data, there are 11 different types of alteration in the modeling space, while there are only 6 alteration types on the surface (Figures 2 and 4b) showing the higher diversity of the alteration in depth. Among different alteration types, five alteration types including argillic, calcitized, phyllic, potassic and silicific show positive contrast and studentized contrast (5) which were used as input binary models to the modeling process. As explained in section 2, the Cu-bearing mineralization zones in the study area were mainly associated with azurite and malachite stockwork veins with minor chalcopyrite as inclusions within quartz. According to the results, the silicific units which involve less than 1% of the modeling space show the



highest contrast and studentized contrast indicating high correlation of this alteration type with the Cu mineralization in the modeling space. The potassic units which involve greater than 65% of the modeling space are in the second place of the highest studentized contrast and third place of the highest contrast which is a low value. It is expected to see a high correlation between the potassic alteration and the Cu mineralization, and a high studentized contrast indicates low uncertainty of these units in terms of the association with the Cu mineralization in the modeling space which fulfills this expectation. The phyllic and calcitized units which respectively involve greater than 9% and less than 1% of the modeling space show low contrast value, but a relatively high studentized contrast value which is much lower than the potassic and silicific units. The argillic units which involve less than 2% of the modeling space, as expected show low contrast and studentized contrast showing weak association with the Cu mineralization in the modeling space.

According to Figure 4c, the rocks located in the modeling space originate from five different sources. Among different types of rock origin, only volcanic rocks show a positive contrast and studentized contrast. This type of rocks occupies more than 87% of the modeling space which is a significant value and shows a high studentized contrast, although the contrast value is low. It implies the low uncertainty of the volcanic rocks in terms of association with the Cu mineralization in the modeling space.

Besides the qualitative geological data, we used the quantitative geochemical data of three elements including Fe, Mo, and Zn which are known as the most important Cu trace elements in the study area. As explained in

section 3.3.1, multiple binary models were created for each element and after determining the proper threshold for creating a binary model of the Cu concentration, the weights of evidence for each binary model of the geochemical elements were investigated through determining a suitable threshold for them. According to Tables 2–4, and maximum studentized contrast obtained for each geochemical element, the best threshold was determined for creating the binary geochemical models. Different trends of contrast and studentized contrast for each geochemical element shown in Figure 11, indicate the errors associated with particular contrast values due to small amount of the data, or due to small volumes. It is obvious that the selected threshold for creating geochemical evidential models maybe far from the known cutoff grade of a specific geochemical element, but the fact is that the aim is to prospect for Cu and these models are only used as an evidence of Cu mineralization.

In this study, we created two probability models including posterior probability and studentized posterior probability models for visualizing the Cu mineralization potential in the target modeling space. It is clear that studentized posterior probability model is more reliable due to the contribution of uncertainty through determining anomalous voxels. The number of anomalous voxels in the posterior probability model which is determined based on the C-V fractal model, is more than three times greater than the number of anomalous voxels in the studentized posterior probability model. We observed that in the spaces where there are few or no borehole inside or near it, the total variance or uncertainty shows a high value which proves the capability of this index for the defined task.

The intersection point in the P-A plot of the posterior probability model

shows 62% of the anomalous voxels of the interpolated Cu concentration were predicted in 38% of the total modeling space. The intersection point in the P-A plot corresponding to the studentized posterior model shows 45% of the anomalous voxels of the interpolated Cu concentration were predicted in 55% of the total modeling space. The main reason for the better results of the posterior probability model is by ignoring high number of voxels due to high values of uncertainty in the studentized posterior probability model. We implemented all the steps of the three-dimensional weights of evidence modeling using the Python scripts which are released for the first time and freely available enclosed to this study. The main advantage of these scripts is that they are simple and easy to understand for any user who has a basic knowledge of the computer programming. Moreover, they can be run fast even by a normal computer. The scripts can be developed in future for other types of the three-dimensional weights of evidence modeling method.

## 6. Conclusions

In this study, we integrated the qualitative geological and quantitative geochemical drilling data obtained from 113 boreholes located on a porphyry Cu deposit in southeast of Iran within Urmia-Dokhtar magmatic arc, through creating a mineral prospectivity model based on 3D weights of evidence. The input evidential models to the modeling process comprise of lithology, alteration and rock origin data in addition to geochemical models including Fe, Mo, and Zn concentration values. Based on the maximum studentized contrast, we determine the thresholds for creating binary models from the continuous geochemical models which are created by interpolating concen-

tration values using an anisotropic inverse distance method. The selected thresholds are not necessarily equal or near to the cutoff grade of the trace element, but help to separate those voxels which are highly correlated with the Cu mineralization.

The final models include posterior probability, total variance that projects the uncertainty, and studentized posterior probability. The anomalous voxels in probability models are determined using the C-V fractal models through finding the suitable threshold for separating anomaly population from the background. The posterior probability model shows better results based on the P-A plots, although the studentized posterior probability model is more reliable due to the lower uncertainty. The results show the efficiency of our method in constructing different geometric models of a specific ore deposit concealed in depth, determining key factors which control the mineralization in the modeling space, identifying potential mineralization and improving the perception of ore genesis.

The mineral prospectivity modeling based on the weights of evidence is highly dependent on the model considered as the target ore body. In future, we aim to use geostatistical methods for creating a more reliable model to consider as the target ore body, because we would be able to provide an uncertainty model beside the model yielded by the interpolation process. In addition, we can decrease the uncertainty in our posterior probability model by adding other exploration data such as geochemical and geophysical models and creating more input evidential models compatible to the metallogenic model of the study area.

## Supplementary data

The Python scripts and a supplementary file containing the weights of evidence and other parameters for the evidential models are available at [https://github.com/intelligent-exploration/3D\\_MPM](https://github.com/intelligent-exploration/3D_MPM).

## References

- Abedi, M., Gholami, A., Norouzi, G.H., 2014. 3D inversion of magnetic data seeking sharp boundaries: A case study for a porphyry copper deposit from Now Chun in central Iran. *Near Surface Geophysics* 12, 657–666. doi:10.3997/1873-0604.2014022.
- Afzal, P., Alghalandis, Y.F., Khakzad, A., Moarefvand, P., Omran, N.R., 2011. Delineation of mineralization zones in porphyry Cu deposits by fractal concentration-volume modeling. *Journal of Geochemical Exploration* 108, 220–232. doi:10.1016/j.gexplo.2011.03.005.
- Agterberg, F.P., Bonham-Carter, G.F., Wright, D.F., 1990. Statistical Pattern Integration for Mineral Exploration, in: Gaal, G., Merriam, D.F. (Eds.), *Computer Applications in Resource Estimation*. Pergamon. *Computers and Geology*, pp. 1–21. doi:10.1016/B978-0-08-037245-7.50006-8.
- ArcGIS Desktop, 2019. ESRI. URL: <https://www.esri.com/en-us/arcgis/about-arcgis/overview>.
- Berberian, F., Berberian, M., 1981. Tectono-Plutonic Episodes in Iran, in: *Zagros Hindu Kush Himalaya Geodynamic Evolution*. American Geophysical Union (AGU), pp. 5–32. doi:10.1029/GD003p0005.

- Bishop, M.M., Fienberg, S.E., Holland, P.W., 1975. Discrete Multivariate Analysis: Theory and Practice. MIT Press.
- Bonham-Carter, G.F., 1994. Geographic Information Systems for Geoscientists: Modeling with GIS.
- Bonham-Carter, G.F., Agterberg, F.P., Wright, D.F., 1989. Weights of evidence modelling: a new approach to mapping mineral potential, in: Agterberg, F.P., Bonham-Carter, G.F. (Eds.), Statistical Applications in the Earth Sciences. Geological Survey of Canada, pp. 171–183.
- Brown, W.M., Gedeon, T.D., Groves, D.I., Barnes, R.G., 2000. Artificial neural networks: a new method for mineral prospectivity mapping. Australian Journal of Earth Sciences 47, 757–770. doi:10.1046/j.1440-0952.2000.00807.x.
- Carranza, E.J.M., 2004. Weights of evidence modeling of mineral potential: a case study using small number of prospects, Abra, Philippines. Natural Resources Research 13, 173–187. doi:10.1023/B:NARR.0000046919.87758.f5.
- Carranza, E.J.M., 2009. Controls on mineral deposit occurrence inferred from analysis of their spatial pattern and spatial association with geological features. Ore Geology Reviews 35, 383–400. doi:10.1016/j.oregeorev.2009.01.001.
- Carranza, E.J.M., Laborte, A.G., 2015. Random forest predictive modeling of mineral prospectivity with small number of prospects and data with

- missing values in Abra (Philippines). *Computers & Geosciences* 74, 60–70. doi:10.1016/j.cageo.2014.10.004.
- Carranza, E.J.M., van Ruitenbeek, F.J.A., Hecker, C., van der Meijde, M., van der Meer, F.D., 2008. Knowledge-guided data-driven evidential belief modeling of mineral prospectivity in Cabo de Gata, SE Spain. *International Journal of Applied Earth Observation and Geoinformation* 10, 374–387. doi:10.1016/j.jag.2008.02.008.
- Carranza, E.J.M., Sadeghi, M., 2010. Predictive mapping of prospectivity and quantitative estimation of undiscovered VMS deposits in Skellefte district (Sweden). *Ore Geology Reviews* 38, 219–241. doi:10.1016/j.oregeorev.2010.02.003.
- Carranza, E.J.M., Woldai, T., Chikambwe, E.M., 2005. Application of data-driven evidential belief functions to prospectivity mapping for aquamarine-bearing pegmatites, Lundazi district, Zambia. *Natural Resources Research* 14, 47–63. doi:10.1007/s11053-005-4678-9.
- Chen, Y., Wu, W., 2017. Mapping mineral prospectivity using an extreme learning machine regression. *Ore Geology Reviews* 80, 200–213. doi:10.1016/j.oregeorev.2016.06.033.
- Cheng, Q., Agterberg, F.P., 1999. Fuzzy weights of evidence method and its application in mineral potential mapping. *Natural Resources Research* 8, 27–35. doi:10.1023/A:1021677510649.
- Fallara, F., Legault, M., Rabeau, O., 2006. 3-D integrated geological mod-

- eling in the Abitibi Subprovince (Québec, Canada): techniques and applications. *Exploration and Mining Geology* 15, 27–43.
- Farahbakhsh, E., Chandra, R., Eslamkish, T., Müller, R.D., 2019. Modeling geochemical anomalies of stream sediment data through a weighted drainage catchment basin method for detecting porphyry Cu-Au mineralization. *Journal of Geochemical Exploration* 204, 12–32. doi:10.1016/j.gexplo.2019.05.003.
- Houlding, S., 1994. *3D Geoscience Modeling: Computer Techniques for Geological Characterization*. Springer.
- Hu, X., Yuan, F., Li, X., Jowitt, S.M., Jia, C., Zhang, M., Zhou, T., 2018. 3D characteristic analysis-based targeting of concealed Kiruna-type Fe oxide-apatite mineralization within the Yangzhuang deposit of the Zhonggu orefield, southern Ningwu volcanic basin, middle-lower Yangtze River metallogenic Belt, China. *Ore Geology Reviews* 92, 240–256. doi:10.1016/j.oregeorev.2017.11.019.
- Jessell, M., Aillères, L., Kemp, E.D., Lindsay, M., Wellmann, F., Hillier, M., Laurent, G., Carmichael, T., Martin, R., 2014. Next Generation Three-Dimensional Geologic Modeling and Inversion, in: *Building Exploration Capability for the 21st Century*, pp. 261–272. doi:10.5382/SP.18.13.
- Joly, A., Porwal, A., McCuaig, T.C., 2012. Exploration targeting for orogenic gold deposits in the Granites-Tanami Orogen: Mineral system analysis, targeting model and prospectivity analysis. *Ore Geology Reviews* 48, 349–383. doi:10.1016/j.oregeorev.2012.05.004.



- Knox-Robinson, C.M., 2000. Vectorial fuzzy logic: a novel technique for enhanced mineral prospectivity mapping, with reference to the orogenic gold mineralisation potential of the Kalgoorlie Terrane, Western Australia. *Australian Journal of Earth Sciences* 47, 929–941. doi:10.1046/j.1440-0952.2000.00816.x.
- Li, N., Song, X., Xiao, K., Li, S., Li, C., Wang, K., 2018. Part II: A demonstration of integrating multiple-scale 3D modelling into GIS- based prospectivity analysis: A case study of the Huayuan-Malichang district , China. *Ore Geology Reviews* 95, 292–305. doi:10.1016/j.oregeorev.2018.02.034.
- Li, X., Yuan, F., Zhang, M., Jia, C., Jowitt, S.M., Ord, A., Zheng, T., Hu, X., Li, Y., 2015. Three-dimensional mineral prospectivity modeling for targeting of concealed mineralization within the Zhonggu iron orefield, Ningwu basin, China. *Ore Geology Reviews* 71, 633–654. doi:10.1016/j.oregeorev.2015.06.001.
- Lindsay, M.D., Aillères, L., Jessell, M.W., de Kemp, E.A., Betts, P.G., 2012. Locating and quantifying geological uncertainty in three-dimensional models: analysis of the Gippsland basin, Southeastern Australia. *Tectonophysics* 546-547, 10–27. doi:10.1016/j.tecto.2012.04.007.
- Liu, L., Li, J., Zhou, R., Sun, T., 2016. 3D modeling of the porphyry-related Dawangding gold deposit in south China: Implications for ore genesis and resources evaluation. *Journal of Geochemical Exploration* 164, 164–185. doi:10.1016/j.gexplo.2015.11.002.

- Lu, Y., Liu, L., Xu, G., 2016. Constraints of deep crustal structures on large deposits in the Cloncurry district, Australia: evidence from spatial analysis. *Ore Geology Reviews* 79, 316–331. doi:10.1016/j.oregeorev.2016.05.022.
- Manap, M.A., Sulaiman, W.N.A., Ramli, M.F., Pradhan, B., Surip, N., 2013. A knowledge-driven GIS modeling technique for groundwater potential mapping at the Upper Langat Basin, Malaysia. *Arabian Journal of Geosciences* 6, 1621–1637. doi:10.1007/s12517-011-0469-2.
- Mao, X., Ren, J., Liu, Z., Chen, J., Tang, L., Deng, H., Bayless, R.C., Yang, B., Wang, M., Liu, C., 2019. Three-dimensional prospectivity modeling of the Jiaojia-type gold deposit, Jiaodong Peninsula, Eastern China: A case study of the Dayingezhuang deposit. *Journal of Geochemical Exploration* 203, 27–44. doi:10.1016/j.gexplo.2019.04.002.
- Nielsen, S.H.H., Cunningham, F., Hay, R., Partington, G., Stokes, M., 2015. 3D prospectivity modelling of orogenic gold in the Marymia Inlier, Western Australia. *Ore Geology Reviews* 71, 578–591. doi:10.1016/j.oregeorev.2015.02.001.
- Omran, J., Agard, P., Whitechurch, H., Benoit, M., Prouteau, G., Jolivet, L., 2008. Arc-magmatism and subduction history beneath the Zagros Mountains, Iran: a new report of adakites and geodynamic consequences. *Lithos* 106, 380–398. doi:10.1016/j.lithos.2008.09.008.
- Payne, C.E., Cunningham, F., Peters, K.J., Nielsen, S., Puccioni, E., Wildman, C., Partington, G.A., 2015. From 2D to 3D: prospectivity modelling

- in the Taupo volcanic zone, New Zealand. *Ore Geology Reviews* 71, 558–577. doi:10.1016/j.oregeorev.2014.11.013.
- Pazand, K., Hezarkhani, A., 2014. The use of the weights-of-evidence modeling technique to predictive porphyry Cu potential mapping in Ahar-Arasbaran zone, Iran. *Arabian Journal of Geosciences* 7, 4191–4201. doi:10.1007/s12517-013-0983-5.
- Porwal, A., Carranza, E.J.M., Hale, M., 2003. Knowledge-driven and data-driven fuzzy models for predictive mineral potential mapping. *Natural Resources Research* 12, 1–25. doi:10.1023/A:1022693220894.
- Porwal, A., González-Álvarez, I., Markwitz, V., McCuaig, T.C., Mamuse, A., 2010. Weights-of-evidence and logistic regression modeling of magmatic nickel sulfide prospectivity in the Yilgarn craton, Western Australia. *Ore Geology Reviews* 38, 184–196. doi:10.1016/j.oregeorev.2010.04.002.
- QGIS Development Team, 2019. QGIS Geographic Information System.
- RockWorks17, 2019a. Software Help Files (Revision 2019.7.30). URL: <https://help.rockware.com/rockworks17/WebHelp/introduction.htm>.
- RockWorks17, 2019b. Software (Revision 2019.7.30). URL: <https://www.rockware.com/product/rockworks/>.
- Rodriguez-Galiano, V., Sanchez-Castillo, M., Chica-Olmo, M., Chica-Rivas, M., 2015. Machine learning predictive models for mineral prospectivity: an evaluation of neural networks, random forest, regression trees and support vector machines. *Ore Geology Reviews* 71, 804–818. doi:10.1016/j.oregeorev.2015.01.001.

- Shishaye, H.A., Tait, D.R., Befus, K.M., Maher, D.T., 2019. An integrated approach for aquifer characterization and groundwater productivity evaluation in the Lake Haramaya watershed, Ethiopia. *Hydrogeology Journal* 27, 2121–2136. doi:10.1007/s10040-019-01956-7.
- Xiao, K., Li, N., Porwal, A., Holden, E.J., Bagas, L., Lu, Y., 2015. GIS-based 3D prospectivity mapping: A case study of Jiama copper-polymetallic deposit in Tibet, China. *Ore Geology Reviews* 71, 611–632. doi:10.1016/j.oregeorev.2015.03.001.
- Xiong, Y., Zuo, R., 2018. GIS-based rare events logistic regression for mineral prospectivity mapping. *Computers & Geosciences* 111, 18–25. doi:10.1016/j.cageo.2017.10.005.
- Yousefi, M., Nykänen, V., 2016. Data-driven logistic-based weighting of geochemical and geological evidence layers in mineral prospectivity mapping. *Journal of Geochemical Exploration* 164, 94–106. doi:10.1016/j.gexplo.2015.10.008.
- Yuan, F., Li, X., Zhang, M., Jowitt, S.M., Jia, C., Zheng, T., Zhou, T., 2014. Three-dimensional weights of evidence-based prospectivity modeling: A case study of the Baixiangshan mining area, Ningwu Basin, Middle and Lower Yangtze Metallogenic Belt, China. *Journal of Geochemical Exploration* 145, 82–97. doi:10.1016/j.gexplo.2014.05.012.
- Zeghouane, H., Allek, K., Kesraoui, M., 2016. GIS-based weights of evidence modeling applied to mineral prospectivity mapping of Sn-W and

- rare metals in Laouni area, Central Hoggar, Algeria. *Arabian Journal of Geosciences* 9, 373. doi:10.1007/s12517-015-2188-6.
- Zuo, R., Carranza, E.J.M., Wang, J., 2016. Spatial analysis and visualization of exploration geochemical data. *Earth-Science Reviews* 158, 9–18. doi:10.1016/j.earscirev.2016.04.006.
- Zuo, R., John, E., Carranza, E.J.M., 2011. Support vector machine: a tool for mapping mineral prospectivity. *Computers & Geosciences* 37, 1967–1975. doi:10.1016/j.cageo.2010.09.014.